

Geochemistry and Petrogenesis of Intracontinental Basaltic Volcanism on the Northwest Arabian Plate, Gaziantep Basin, Southeast Anatolia, Turkey

Sevcan KÜRÜM^{1,*}, Abdurrahman BÖLÜCÜ² and Melek URAL¹

¹ Department of Geological Engineering, University of Firat, 23110 Elazığ, Turkey

² Institute of Science and Technology, University of Firat, 23110 Elazığ, Turkey

Abstract: Volcanism along the northwest boundary of the Arabian Plate found in the Gaziantep Basin, southeast Turkey, is of Miocene age and is of alkaline and calc-alkaline basic composition. The rare earth element data for both compositional series indicates spinel–peridotite source areas. The rare earth and trace elements of the alkaline lavas originate from a highly primitive and slightly contaminated asthenospheric mantle; those of the calc-alkaline lavas originate from a highly heterogeneous, asthenospheric, and lithospheric mantle source. Partial melting and magmatic differentiation processes played a role in the formation of the petrological features of these volcanics. These rocks form two groups on the basis of their $^{87}\text{Sr}/^{86}\text{Sr}$ and $^{143}\text{Nd}/^{144}\text{Nd}$ isotopic compositions in addition to their classifications based on their chemical compositions (alkaline and calc-alkaline). These isotopic differences indicate a dissimilar parental magma. Therefore, high Nd isotope samples imply a previously formed and highly primitive mantle whereas low Nd isotope samples may indicate comparable partial melting of an enriched heterogeneous shallow mantle. Other isotopic changes that do not conform to the chemical features of these lavas are partly related to the various tectonic events of the region, such as the Dead Sea Fault System and the Bitlis Suture Zone.

Key words: petrography, geochemistry, isotopes, basaltic volcanism, Arabian Plate, Turkey

1 Introduction

The Tauride–Anatolian plate is composed of different oceanic and continental areas in a region where Alpine orogenesis has been active in the geological processes (Göncüoğlu et al., 1997). East–Southwest Anatolia is an important region that presents a complex tectonic mosaic of this Alpine orogenic period (Okay, 2008). The geodynamic evolution of the region is related to the relative movements of three large plates: Eurasian, African, and Arabian (Dilek and Altunkaynak, 2009). The main orogenic event in the region is considered to be controlled by the closure of the different branches of Neotethys Ocean (Şengör and Yılmaz, 1981). In Southeast Anatolia, which forms the northern part of Arabian platform, two main Alpine tectonic zones are found: the Bitlis Suture Zone (SE Anatolian Fold/Thrust Belt) and the SE Anatolia Zone/Autochthonous (Göncüoğlu, 2010). The Bitlis Suture Zone is considered the region where the Arabian and Anatolian plates collided along the Bitlis–

Zagros collision belt during the Late Oligocene–Early Miocene (Perinçek, 1979; Şengör and Kidd, 1979; Şengör et al., 1985; Yılmaz, 1993; Yiğitbaş and Yılmaz, 1996; Dilek and Altunkaynak, 2009; Kuşcu et al., 2010; McQuarrie et al., 2003) (Fig. 1a). Therefore, the neotectonics of the region is associated with the history and geometry of the southern branch of Neotethys (Stampfli, 2000; Moix et al., 2008).

The collision along the northern boundary of the Arabian Plate commenced during the Middle–Late Eocene, and the velocity of convergence between the Afro–Arabian and Eurasian plates decreased during this process (Çoban, 2007; Ma et al., 2013). As a result of these complex tectonic relationships, widespread volcanic activities within the Arabian Plate have occurred from the Neogene to recent times (Fig. 1b) (Çapan et al., 1987; Giannerini et al., 1988; Garfunkel, 1989; Heimann and Ron, 1993; Coşkun and Coşkun, 2000; İlani et al., 2001; Alpaslan, 2007; Ma et al., 2013). The magmatic activity in the region occurred contemporaneously with the tectonic events that resulted from the movement of the Arabian Plate toward the north during the Cenozoic period

* Corresponding author. E-mail: skurum@firat.edu.tr

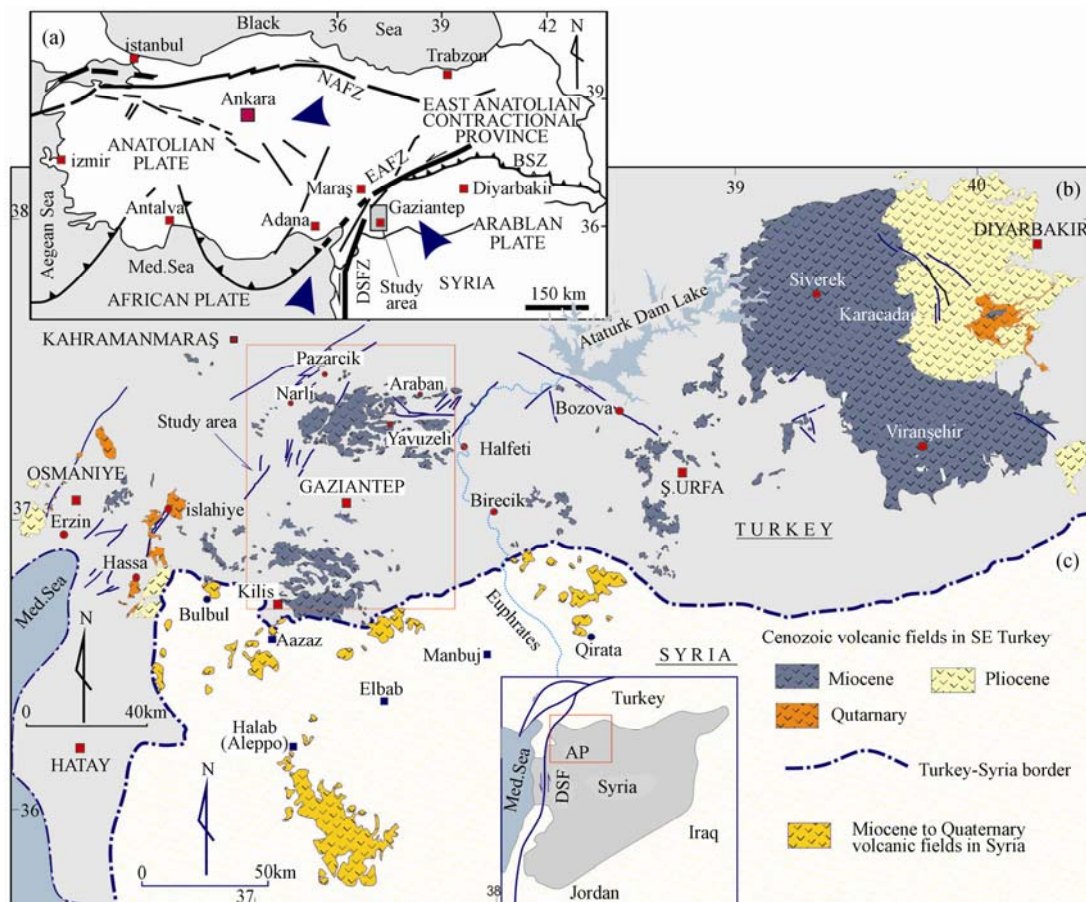


Fig. 1. (a), Simplified geotectonic map of Turkey showing the major Neotectonic elements and the direction of tectonic transportation (from Göncüoğlu, 2010); (b), geological map of the study area (modified from MTA, 2002); (c), location map of northwestern Syrian volcanic fields. The inset shows the NW part of the Arabian peninsula with active fault zones (simplified from Krienitz et al., 2006). NAFZ - North Anatolian Transform Fault; EAFZ - East Anatolian Transform Fault; BSZ - Bitlis Suture Zone; DSFZ - Dead Sea Fault Zone; AP - Aleppo Plateau.

(Giannerini et al., 1988; Rukieh et al., 2005). The Dead Sea Fault Zone (DSFZ), which determines the boundary between the African and Arabian-Anatolian plates, is divided into different segments. South Turkey is important in this respect (Fig. 1). Correspondingly, a widespread alkaline magmatic evolution occurred during the Eocene-Oligocene transition in the Afro-Arabian Plate (Libya, Jordan, and Syria; Lustrino and Wilson, 2007).

During the Middle Miocene, the Arabian Plate diverged from the African Plate along the left strike slip DSFZ and the northerly relative movement toward Eurasia continued (Yürür and Chorowicz, 1998). For this reason, crustal shortening and thickening are common in Eastern Anatolia (Şengör et al., 1985; Dewey et al., 1986).

In the same process, the movement of the Arabian Plate to the north relative to Eurasia resulted in a widespread post-collisional magmatism and crustal shortening and thickening in East Anatolia (Taymaz et al., 2007; Allen and Armstrong 2008; Frizon De Lamotte et al., 2011). This volcanic activity occurs in three phases (Yılmaz et

al., 1987): in the first phase, which started immediately after the collapse, there was weak alkaline volcanism such as the Solhan volcanites; volcanism was rich in K and Ca in the second phase, which started in the Late Miocene-Early Pliocene; and alkaline basaltic products were developed in the third phase, which started in Pleistocene-Quaternary.

A few young volcanic suites have been found in the vicinity of the study area in Turkey (Amik Basin, Karasu Basin, Osmaniye region). They erupted through the extension zones developed along the DSFZ with NE-SW strike separating the African-Arabian and Anatolian plates and resulted from the lithospheric tension that has continued since the Late Pliocene (Fig. 1b) (Parlak et al., 1998, 2000; Yürür and Chorowicz, 1998; Coşkun and Coşkun, 2000; Yüce et al., 2014). One of the similar examples due to continental events in the world is observed in the Tibetan Plateau (Lai, 2016).

On the basis of the previous investigations, this study aims to interpret the source characteristics, magmatic

processes, and geodynamic evolution of the Miocene volcanic rocks found in the Gaziantep Basin, which spans the northwest boundary of Arabian Plate.

2 Regional Volcanism and Local Geology

The basement rocks of the study area in the Gaziantep Basin are differentiated into Paleozoic and Mesozoic formations (Coşkun and Coşkun, 2000). The Paleozoic is represented by sedimentary rocks formed in different depositional environments, whereas the Mesozoic is represented by shallow to deep marine facies and ophiolites (Coşkun and Coşkun, 2000). The Late Cretaceous ophiolites (Koçali–Karadut Complex) formed as a result of the convergence between the African–Arabian and Eurasian plates (Alpaslan, 2007). The Tertiary (Paleocene–Oligocene) units essentially comprise shallow marine carbonates (Ulu et al., 1991; Coşkun and Coşkun, 2000).

As mentioned earlier, the geological evolution of the rock associations in Southeast Anatolia was controlled by the evolution of Tethys and by tectonic events. Despite the occurrence of active tectonism in the region, the Arabian Platform is relatively stable tectonically. The presence of Triassic to Tertiary carbonates, clastic rocks, fine shale, and siltstone facies is indicative of this fact (Coşkun and Coşkun, 2000).

The volcanism in Syria, to the south of the study area, is related to different tectonic events, such as replacements along the DSFZ or slab breakoff under the Bitlis Suture Zone (Krienitz et al., 2009). The volcanism at the vicinity of the Turkish border (Fig. 1c) is formed by a few different volcanic phases during Miocene–Quaternary periods (Krienitz et al., 2009). The latest phase of the volcanism (post-3 Ma) in northern Syria can be correlated with the Karacadağ volcanic region (2.7 ± 0.2 Ma to 101 ± 18 ka) (Bridgland et al., 2007). However, when the volcanic activity in the Karacadağ region was in its peak, no equivalent volcanism occurred in North Syria (Demir et al., 2007). The Cenozoic volcanism in the middle and eastern parts of Syria is of Upper Eocene–Holocene age (~ 40 – 0.0005 Ma) and comprises alkaline mafic rocks, transitional–tholeiitic basalts, and basaltic andesites. These volcanic suites with geochemical differences form two phases; the first is in the age range of ~ 25 – 5 Ma, and the second is from ~ 5 Ma to recent (Lustrino and Sharkov, 2006). However, the age of the volcanism in Syria is highly debated. For example, Ponikarov et al. (1963) indicated that the majority of the volcanic units in Syria are of Late Pliocene age. By contrast, Krienitz et al. (2006) reported that the lavas from the Bülbül region to northwest Syria, near the Turkish border are of 10 to 12

Mya and the Qirata lavas to the northeast of the country are of Quaternary age (Fig. 1c). Similarly, Ma et al. (2013) agreed that the Miocene volcanites were formed in two different phases (Phase 1, 19–18 Ma and Phase 2, ~ 13.5 – 12 Ma) and that they were active before the formation of the Dead Sea Fault System. These Miocene volcanic lavas are usually of “aa type” and are found as lava flows thinner than <10 m; however, their thickness may reach 350 m (Krienitz et al., 2006). The chemical and isotopic data obtained from these lavas indicate the effects of crustal assimilation and fractional crystallization (FC). Despite the effect of FC and assimilation (AFC) processes, the two phases display differences owing to source heterogeneity (Ma et al., 2013).

The northern border of the Arabian Plate, including the study area, gradually uplifted during the Early–Middle Miocene, and became a continental basin and within the volcanic sequence, with basaltic rocks as the first ones to form (Ulu et al., 1991). The lavas in the region possess thicknesses of more than 100 m, and their ages vary from Early–Middle Miocene to recent (Fig. 1b) (Çapan et al., 1987; Parlak et al., 1998; Arger et al., 2000; Rojay et al., 2001; Yurtmen et al., 2000; Tatar et al., 2004; Bridgland et al., 2007; Lustrino et al., 2010). Four basaltic lava flows are also found (Alpaslan, 2007). The Siverek/Karacadağ Plateau basalts to the east of the study area form two groups of volcanic sequences of alkaline nature (Bridgland et al., 2007; Lustrino et al., 2010; Ekici et al., 2012) (Fig. 1b). The differences in trace elements between the two groups, which originated from a lherzolitic source, cannot be explained by either FC or crustal contamination according to Ekici et al. (2012). The studies have indicated that the Siverek Plateau basalts were formed at the same time as the magmatism to the north of Syria and in the Karasu Valley and that contamination with crustal rocks is small.

2.1 Field and petrographic characteristics

In the Gaziantep Basin, the volcanic rocks that spread around Narlı–Yavuzeli to the north and around Kilis to the south overlie Oligocene limestones that form the basement of the basin (Fig. 1). Although these volcanic rocks are usually found as lava flows of basaltic composition, their agglomerates and tuffs support them in the lower part. The lavas are usually massive and appear as rounded blocks on the surface. However, thickly layered, fine grained, and vesicular lavas with calcite fillings may also be present locally. The surfaces of the lavas are dark reddish to brownish-dark grayish in color and are mossy, with their freshly broken surfaces blackish-dark grayish in color.

The entire lava flows in the study area display similar mineralogical properties. However, size differences in the

minerals result in textural differences. In the north around Narlı–Yavuzeli, the lava flows are finely crystallized and display intergranular, porphyritic-glomeroporphyritic, and vesicular textures (Fig. 2a–d). By contrast, the lavas to the south with similar mineralogical composition present significantly large crystals, doleritic texture, and oriented minerals (Fig. 2e–g). The main mineral phase of samples with a phenocryst index ratio smaller than 25% is composed of plagioclase, olivine, and pyroxene, and their main phenocryst phase mainly comprises olivine. Apart from opaque minerals, secondary calcite is found in the

hollow spaces between the minerals. Specifically, samples with fine crystals comprise the plagioclases and pyroxenes as micro-phenocrysts (Fig. 2), whereas samples with large crystals contain long plagioclases and pyroxenes as phenocrysts along with olivines. The olivine and pyroxene crystals are the mafic mineral components of these rocks; their abundances are variable, but olivine is usually dominant (Fig. 2). Given that olivine is found as phenocrysts, its presence ratio is higher than that of pyroxenes.

The plagioclases are the most abundant mineral in all

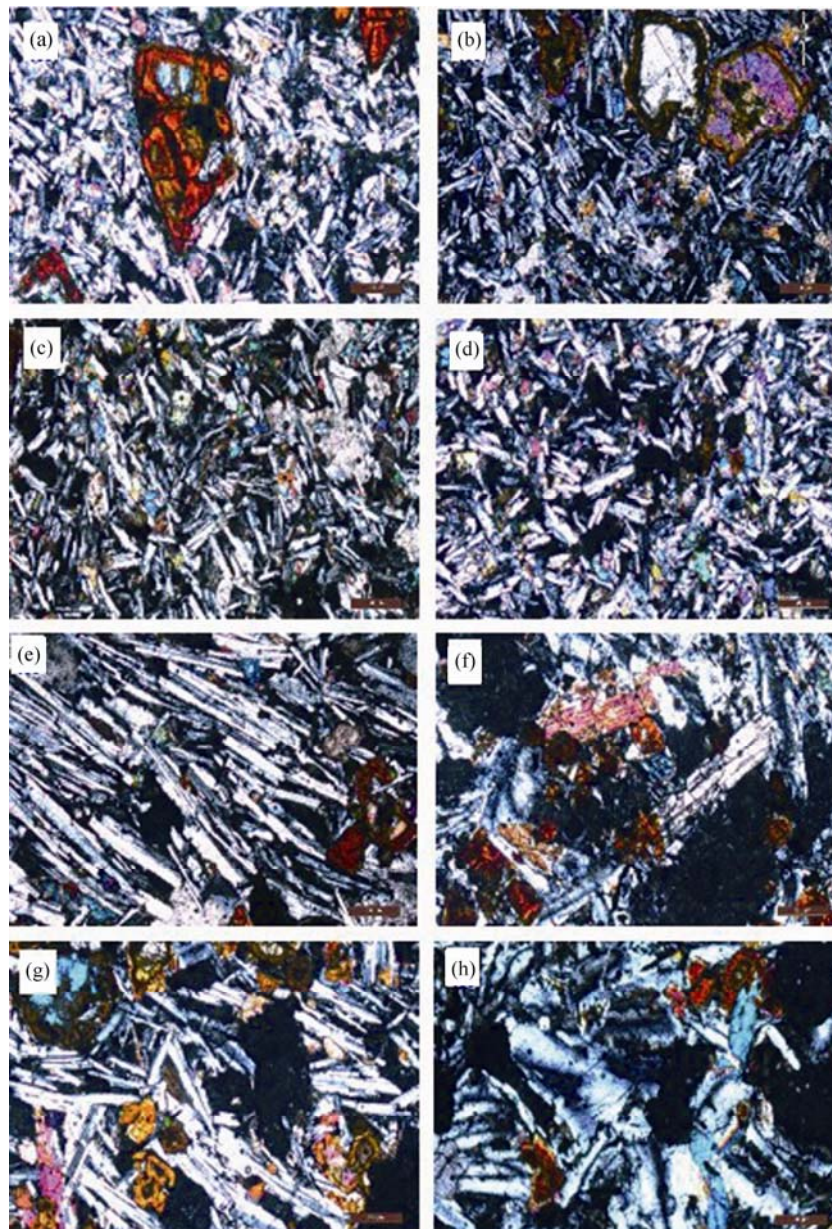


Fig. 2. Photomicrographs showing typical textures of the volcanic rocks in the study area. All photographs are in cross-polarized light. (a) and (b), Basalt with euhedral to subhedral olivine phenocrysts formed by iddingsitization in a holocrystalline (intergranular to sub-ophitic) groundmass (samples A2, A14); (c), and (d), Basalt with olivine plagioclase and pyroxene phenocryst in a fine-grained hypocrySTALLINE groundmass (samples A3, A9); (e), Tabular plagioclase crystals with flow orientation (sample A20); (f), Basalt with euhedral to subhedral pyroxene phenocrysts in a holocrystalline groundmass (sample A18); (g), Basalt with euhedral to subhedral and clinopyroxene-rim olivine phenocrysts in a holocrystalline groundmass (sample A-26); (h), Plagioclase with zoning (sample A29).

samples. However, their sizes vary depending on the texture. They are found as small crystals of prismatic laths that show zonation and twinning in finely textured rocks. In the rocks with large crystals, plagioclases are also large and appear as prismatic laths that display zonation and twinning and form a holocrystalline. Apart from the alterations observed in the rocks in general, plagioclases are unaltered.

Olivine is usually found as euhedral and subhedral phenocrystals in these rocks. The major characteristic feature of the olivine minerals found in these rocks is iddingsitization. The majority of phenocrystals are iddingsitized, and in some cases, they are iddingsitized along their margins and joints. However, a few altered olivine crystals are found in some samples. The corona texture found in olivines in some samples is important from the petrographic point of view, because it indicates magma mixing.

The other mafic components of these basaltic lavas are clinopyroxenes that show vivid polarization colors (presumably augite) and appear as small, unehedral, cleaved, and unaltered crystals.

In all samples, carbonation is formed between the main minerals. In some samples, plagioclase microliths are found as inclusions in the carbonate crystals. Carbonate crystallization does not form into vesicles, and this fact indicates that surface alteration is unimportant.

3 Analytical Methods

The representative rock samples were collected during field work for petrographic and whole-rock geochemical

analyses. Thin sections (37) used for the petrographic studies were prepared at the thin-section laboratory of the Geological Engineering department, Pamukkale University, Denizli, Turkey.

Whole-rock chemical analyses have been performed at the ACME Laboratories and at the ACT-Labs by ICP-AES (Inductively Coupled Plasma Atomic Emission Spectroscopy) for major and some trace elements and ICP-MS (Inductively Coupled Plasma Mass Spectrometry) for rare earth elements in Vancouver (Canada). 0.2 g of rock-powder was fused with 1.5 g LiBO₂ and dissolved in 100 ml 5% HNO₃ for the major and trace-element analyses. Loss on ignition (LOI) was determined on the dried samples heated to a temperature of 1000°C. REE analyses were performed by ICP-MS at ACME. Detection limits ranged from 0.01wt% to 0.1wt% for major oxides, from 0.1 to 10 ppm for trace elements, and from 0.01 to 0.5 ppm for REE.

The Sr and Nd isotope geochemical measurements were performed by the TRITON Thermal Ionization Mass Spectrometer (Thermo-Fisher) at the Radiogenic Isotope Laboratory in METU (Middle East Technical University) Central Laboratories (Ankara, Turkey), following the procedure described in Köksal and Gönçüoğlu (2008), and uncertainties are in the 2 sigma level.

4 Geochemical Discriminations

The results of the chemical analyses and normative CIPW compositions of the 21 studied samples are given in Table 1, and the results of the trace and REE analyses are presented in Table 2. The loss on ignition (LOI) ratios of

Table 1 Major element (wt%) and normative minerals data of Miocene alkaline and calc-alkaline lavas analyzed in this study

Sample	calc-alkaline basalts															alkaline basalts					
	A1	A3	A8	A11	A12	A15	A17	A19	A22	A24	A25	A26	A28	A29	A30	A5	A9	A14	A16	A20	A31
SiO ₂	51.75	52.00	51.39	51.15	49.71	52.05	52.29	51.56	51.39	52.35	51.07	52.11	52.12	52.06	52.05	45.76	44.60	43.30	45.46	43.72	45.05
Al ₂ O ₃	13.90	14.19	13.86	14.29	13.83	14.10	14.21	13.78	13.84	14.06	13.81	14.11	14.00	13.99	13.99	14.30	14.12	13.95	14.35	14.13	14.35
Fe ₂ O ₃	11.14	11.24	11.05	11.58	11.60	11.19	11.40	10.83	10.90	11.01	10.88	11.09	11.00	11.00	10.79	12.24	11.98	11.74	12.03	11.88	12.21
MgO	7.73	7.94	7.78	7.16	8.40	7.94	7.44	7.93	7.89	7.98	7.85	7.86	7.94	7.95	7.95	7.83	7.60	6.57	7.66	6.19	7.69
CaO	8.24	7.75	8.65	8.51	8.88	7.76	7.92	8.44	8.54	7.88	8.65	7.86	7.89	7.84	8.06	10.54	11.34	12.47	10.94	12.28	10.67
Na ₂ O	3.01	3.06	3.04	3.14	3.07	3.08	3.04	2.99	2.98	3.04	2.98	3.06	3.04	3.03	2.99	3.15	3.13	2.91	3.01	2.84	3.10
K ₂ O	0.93	0.94	0.94	0.92	0.74	0.96	1.00	0.93	0.93	0.93	0.94	0.95	0.94	0.95	0.92	1.10	1.13	1.10	1.09	1.10	1.11
TiO ₂	1.65	1.65	1.66	1.52	1.55	1.67	1.53	1.63	1.63	1.69	1.62	1.66	1.69	1.69	1.68	1.74	1.75	1.72	1.73	1.75	1.79
P ₂ O ₅	0.26	0.26	0.26	0.23	0.23	0.27	0.20	0.25	0.26	0.27	0.25	0.26	0.25	0.26	0.25	0.46	0.48	0.48	0.47	0.50	0.49
MnO	0.15	0.14	0.14	0.15	0.14	0.14	0.14	0.14	0.14	0.14	0.14	0.14	0.14	0.14	0.14	0.16	0.16	0.16	0.16	0.16	0.16
LOI	1.0	0.6	1.0	1.1	1.6	0.6	0.6	1.3	1.3	0.4	1.6	0.7	0.7	0.8	0.9	2.4	3.4	5.3	2.8	5.2	3.1
Sum	99.82	99.81	99.82	99.82	99.84	99.81	99.84	99.82	99.83	99.83	99.82	99.82	99.83	99.82	99.82	99.77	99.77	99.76	99.77	99.77	99.76
Normative minerals (CIPW)																					
Q	2.94	2.93	1.96	1.76	-	2.91	3.44	2.50	2.28	3.41	1.88	3.12	3.21	3.23	3.33	-	-	-	-	-	-
Or	5.50	5.56	5.56	5.44	4.37	5.67	5.91	5.50	5.50	5.50	5.56	5.61	5.56	5.61	5.44	6.50	6.68	6.50	6.44	6.50	6.56
Ab	25.47	25.89	25.72	26.57	25.98	26.06	25.72	25.30	25.22	25.72	25.22	25.89	25.72	25.64	25.30	20.92	16.12	12.10	19.75	14.47	19.38
An	21.67	22.21	21.40	22.18	21.77	21.81	22.17	21.43	21.64	21.97	21.53	21.96	21.78	21.77	22.03	21.63	21.14	21.75	22.42	22.56	21.96
Ne	-	-	-	-	-	-	-	-	-	-	-	-	-	-	-	3.11	5.62	6.79	3.10	5.18	3.71
Di	14.07	11.68	15.92	14.95	16.70	11.98	12.73	15.09	15.27	12.32	15.85	12.32	12.62	12.38	13.09	22.27	25.76	29.87	23.18	28.41	22.37
Hy	19.28	21.01	18.41	17.98	17.68	20.79	19.57	19.06	18.92	20.55	18.54	20.37	20.30	20.44	19.95	-	-	-	-	-	-
Ol	-	-	-	-	1.82	-	-	-	-	-	-	-	-	-	-	11.78	10.00	6.60	11.06	6.46	11.42
Mt	16.15	16.30	16.02	16.79	16.82	16.22	16.53	15.70	15.80	15.96	15.77	16.08	15.95	15.95	15.64	17.75	17.37	17.02	17.44	17.22	17.70
Il	3.13	3.13	3.15	2.89	2.94	3.17	2.91	3.10	3.10	3.21	3.08	3.15	3.21	3.21	3.19	3.31	3.32	3.27	3.29	3.32	3.40
Ap	0.60	0.60	0.60	0.53	0.53	0.63	0.46	0.58	0.60	0.63	0.58	0.60	0.58	0.60	0.58	1.07	1.11	1.11	1.09	1.16	1.14
Mg*	52.37	52.82	52.73	49.49	53.43	52.93	50.84	53.70	53.42	53.46	53.35	52.90	53.35	53.38	53.86	50.34	50.13	46.99	50.22	45.23	49.95

the samples collected from the study area are <3 wt% (except for four samples). This property indicates that these rocks are unaffected by hydrothermal alteration. The samples with high LOI ratios exhibit similar K_2O and U concentrations to those of the rest of the samples (Tables 1–2). The main oxide values are close to one another, as shown in the table. The SiO_2 values also range in a narrow interval of 43.30%–53.35% and represent rocks with basic composition (Fig. 3a). Although the SiO_2 contents of the

samples range in such a narrow interval (Fig. 3a), the samples are concentrated in two areas. Given that several large ion lithophile elements (LILE) are mobile (Floyd and Winchester, 1975), using these elements in the diagrams should be carefully reconsidered. Accordingly, the samples are reclassified using comparably immobile elements, such as Ti, Zr, Nb, and Y (HFSE) (Fig. 3b, Winchester and Floyd, 1977). Similar to those in the alkaline silica diagram (Fig. 3a), samples in this diagram

Table 2 Trace element (ppm) and some of the element ratio of Miocene alkaline and calc-alkaline lavas analyzed in this study

Sample	calc-alkaline basalts															alkaline basalts					
	A1	A3	A8	A11	A12	A15	A17	A19	A22	A24	A25	A26	A28	A29	A30	A5	A9	A14	A16	A20	A31
Ni	190	191	187	192	240	192	186	187	199	200	183	184	192	193	190	194	194	175	191	183	194
Sc	19	19	19	19	18	19	18	19	18	19	18	19	19	19	19	21	21	20	21	20	21
Ba	176	201	192	285	182	184	207	184	191	191	190	189	190	185	186	257	269	283	272	299	270
Co	43.8	43.3	40.1	48.9	50.1	42.9	46.1	41.9	41.0	43.5	42.5	43.7	43.4	42.4	41.4	49.6	53.7	49.6	51.6	52.0	51.7
Cs	0.6	0.6	0.5	0.5	0.2	0.6	0.6	0.6	0.5	0.5	0.5	0.6	0.5	0.3	0.3	0.3	0.4	0.3	0.3	0.3	0.3
Ga	19.6	21.1	18.8	20.5	18.8	18.3	19.9	20.1	18.8	18.5	18.9	20.3	19.1	19.6	18.9	18.5	19.3	17.8	17.0	18.2	17.5
Hf	3.4	3.3	3.1	2.6	2.5	3.9	2.8	3.6	3.1	3.0	3.4	3.3	3.1	3.9	2.9	3.7	3.7	3.7	3.0	3.6	3.4
Nb	13.5	15.0	14.2	11.1	13.4	15.4	11.0	15.0	13.9	14.5	14.3	15.2	14.6	16.2	13.9	29.3	31.3	30.8	31.7	31.0	33.9
Rb	19.3	20.0	19.5	20.7	12.6	20.3	24.2	20.6	20.0	20.1	20.0	20.5	20.2	19.7	19.9	14.5	15.0	13.4	14.0	12.5	14.5
Sr	310	326	323	285	289	338	276	336	322	322	326	341	327	330	323	573	635	627	629	615	645
Ta	1.2	1.0	0.9	0.8	1.0	0.9	0.8	0.9	0.9	1.1	1.0	1.0	1.0	1.0	0.9	1.6	1.9	1.7	1.8	1.8	1.9
Th	2.6	2.7	2.6	1.9	2.0	2.8	2.3	2.7	2.7	2.7	2.5	2.9	2.8	2.5	2.5	3.1	3.1	3.2	3.4	3.5	3.2
U	0.7	0.8	0.7	0.8	0.7	0.6	0.9	0.8	0.7	0.7	0.7	0.8	0.7	0.8	0.8	0.9	0.9	0.9	0.9	0.9	1.1
V	161	170	163	180	167	176	172	172	167	166	167	182	168	164	169	176	172	180	178	176	176
W	0.6	<0.5	<0.5	<0.5	<0.5	2.0	1.6	<0.5	<0.5	<0.5	<0.5	0.7	<0.5	0.6	<0.5	0.9	0.6	<0.5	0.5	2.8	<0.5
Zr	117	126	121	103	105	130	106	127	121	123	121	127	128	126	127	138.6	146.6	144.5	143.9	144.6	145.0
Y	18.9	20.0	18.7	18.2	20.0	20.3	18.7	19.0	18.5	19.8	18.9	21.0	19.7	19.8	19.8	17.3	19.3	19.2	18.5	18.5	18.6
La	15.8	17.3	17.0	12.5	14.0	17.1	12.6	15.8	16.0	17.3	16.1	17.0	15.9	16.2	16.3	27.0	28.9	29.0	28.6	29.2	28.9
Ce	31.9	35.8	32.3	25.0	28.0	35.1	25.5	33.4	33.4	33.3	32.7	34.7	33.8	33.5	33.7	51.0	55.0	52.9	54.7	54.1	53.7
Pr	3.81	4.19	4.00	3.08	3.43	3.98	3.08	3.97	3.95	4.03	3.88	4.06	3.88	3.92	3.93	5.53	5.92	5.80	5.80	5.75	5.91
Nd	16.6	17.6	16.2	13.3	15.1	17.2	13.0	17.7	17.3	16.9	17.1	18.6	16.4	17.3	17.4	22.1	23.1	22.0	23.8	22.8	22.4
Sm	3.97	4.06	3.89	3.68	3.55	4.19	3.61	3.92	4.15	4.21	4.05	4.42	4.13	4.21	4.25	4.74	4.91	4.97	4.75	4.69	4.76
Eu	1.24	1.41	1.41	1.20	1.27	1.40	1.16	1.49	1.38	1.45	1.34	1.45	1.34	1.41	1.42	1.57	1.66	1.65	1.67	1.67	1.68
Gd	4.40	4.98	4.50	4.02	4.10	4.60	4.24	4.61	4.71	4.79	4.34	4.83	4.41	4.59	4.60	4.80	4.88	4.71	4.82	4.71	4.88
Tb	0.64	0.70	0.68	0.64	0.61	0.68	0.66	0.68	0.67	0.69	0.67	0.71	0.68	0.69	0.69	0.68	0.68	0.68	0.71	0.67	0.67
Dy	3.86	4.07	4.11	3.61	3.39	4.13	3.92	4.01	3.83	4.11	3.93	4.00	3.78	3.93	3.94	4.07	3.99	3.84	3.93	3.90	3.78
Ho	0.73	0.75	0.70	0.70	0.73	0.75	0.74	0.76	0.72	0.75	0.77	0.81	0.71	0.75	0.75	0.67	0.67	0.69	0.72	0.73	0.77
Er	1.61	1.89	1.96	1.76	1.78	1.90	1.95	1.88	1.93	2.16	1.96	1.92	1.77	1.86	1.84	1.78	1.95	1.86	1.96	1.91	1.79
Tm	0.25	0.27	0.26	0.26	0.25	0.26	0.26	0.29	0.24	0.26	0.27	0.28	0.26	0.26	0.28	0.26	0.26	0.27	0.25	0.26	0.27
Yb	1.57	1.65	1.61	1.59	1.51	1.57	1.54	1.68	1.58	1.50	1.59	1.75	1.57	1.53	1.43	1.52	1.50	1.68	1.54	1.50	1.55
Lu	0.21	0.26	0.24	0.22	0.24	0.23	0.23	0.21	0.23	0.24	0.23	0.25	0.24	0.23	0.24	0.23	0.21	0.21	0.22	0.24	0.24

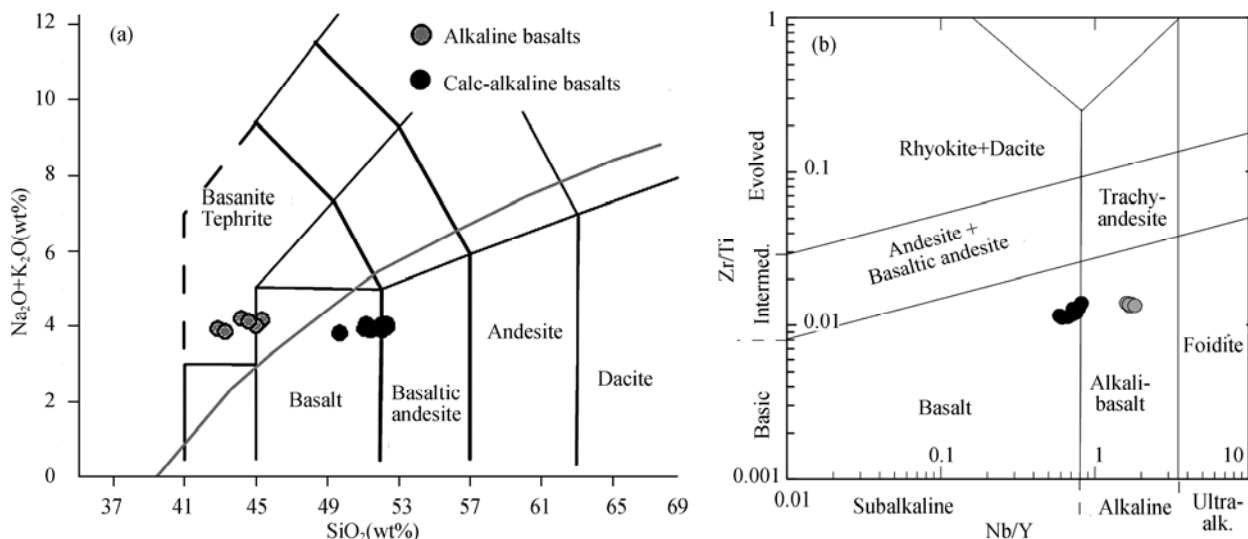


Fig. 3. Classification of the Miocene volcanic rocks in the study area, southeastern Turkey, using nomenclature diagrams. (a), Total alkali-silica of Le Bas et al. (1986); (b), Nb/Y- Zr/Ti by Winchester and Floyd (1977).

are also divided into two groups. The total alkaline contents of all the samples are the same; their silica contents differ, and samples with low silica contents are highly alkaline in nature (Fig. 3a). A similar situation is observed in Zr/Ti and Nb/Y ratios (Fig. 3b). The samples with low Nb/Y ratios are sub-alkaline in nature, whereas those with high Nb/Y ratios are alkaline. These differences in the discrimination diagrams indicate that the volcanic rocks of the study area possess two different compositions: strongly basic and alkaline (1) and weakly basic and calc-alkaline (2) (Fig. 3b). No petrographic difference exists between the two series of rocks, but

samples with alkaline composition contain normative nepheline (Table 1).

The MgO contents of the samples vary between 6.19% and 8.40% with a narrow interval. Harker diagrams were drawn (Figs. 4–5) to analyze the main oxide and change in trace elements along with MgO. The alkaline and calc-alkaline rock series display different behaviors with respect to MgO change in terms of main oxides, except for Al_2O_3 , SiO_2 , and Na_2O (Fig. 4). For example, K_2O , TiO_2 , and P_2O_5 values do not display any trend in the alkaline samples, but they display a weak positive trend in the calc-alkaline samples. Fe_2O_3 presents different distributions in

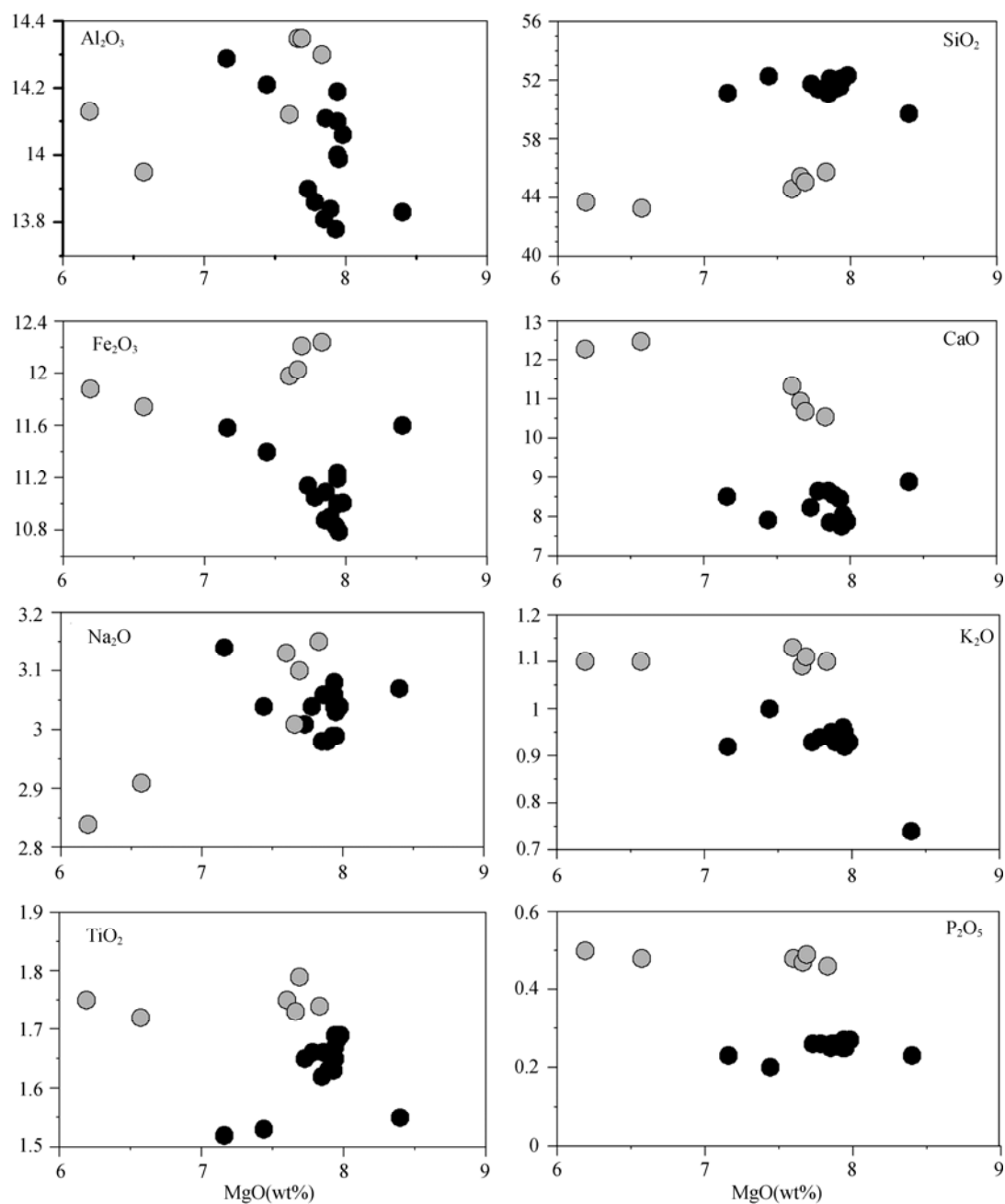


Fig. 4. Selected major elements vs MgO (wt%) diagrams. References as in Figure 3.

both groups and shows positive and negative trends in the alkaline and calc-alkaline samples, respectively. By contrast, CaO shows a negative trend in the alkaline samples and no changes in the calc-alkaline samples. The abundance ratios of the main elements are clearly observed in the Harker diagrams. According to these diagrams, only Na₂O is the same in both series of rocks. Furthermore, all the elements, except SiO₂, are significantly abundant in the samples with alkaline composition.

Although these distributions in both groups of samples indicate different degrees of FC, they predominantly imply a fractionation in the ferromagnesian minerals. In particular, the decrease in MgO contents with the increase in Na₂O and K₂O contents in the calc-alkaline samples indicates the crystallization of Na- and K-bearing minerals, such as amphibole, biotite, Na-plagioclase, and K-feldspars. The transitional element Ni conforms to the decrease in MgO (Fig. 5), and this fact indicates the abundance of ferromagnesian minerals that conform to the main element distributions and the fractionation of ilmenite and other oxides during the early phase. Unlike Ni, the negative anomaly of Co with MgO indicates its accompanying crystallization after attaining sufficient abundance. In addition, its ratio is high in the samples of alkaline composition as expected. The number of incompatible elements increases with the magmatic differentiation degree of acidic magma. This feature is used to determine the evolution of magmatic rocks (Pearce, 1983; Harris et al., 1999). Th and Zr, which are highly incompatible elements, show similar behaviors and

distributions in these lavas of basic composition. For example, the two elements show no trend depending on MgO change in the alkaline rocks, and they display a positive trend in the calc-alkaline rocks. These elements are highly differentiated in the calc-alkaline rocks, and this fact may be explained by very fast crystallization and not by normal fractionation.

The primitive mantle-normalized trace-element patterns of the samples and the reference values of the Upper Continental Crust (UCC), Lower Continental Crust (LCC), Ocean Island *Basalts* (OIB), and Bulk Continental Crust (BCC) are presented in Fig. 6a. The LILE and HFS elements (e.g., Th and U) show similar behaviors in both groups of rocks. Incompatible elements, such as Ta, Nb, La, Ce, and Sr, show a prominent positive trend in the alkaline samples. By contrast, Nb shows negative trend in the calc-alkaline samples. The negative anomaly of Nb in the calc-alkaline samples indicates the existence of a subduction component in the mantle source. According to the diagram, both groups of rocks conform locally to the reference data in general. However, all the samples conform highly to the BCC data.

In the chondrite-normalized multi-element diagram (Fig. 6b), LREEs, such as La, Ce, Pr, and Nd, are enriched in the alkaline samples. However, the enrichment ratios gradually decrease from La toward Nd. After Gd, both series of samples are similar. The flat distribution of HREEs toward the end indicates moderate fractionation and lack of garnet in the source. This distribution also shows that the main magma was formed in the lithospheric mantle (in spinel peridotite) at shallow depth. No Eu

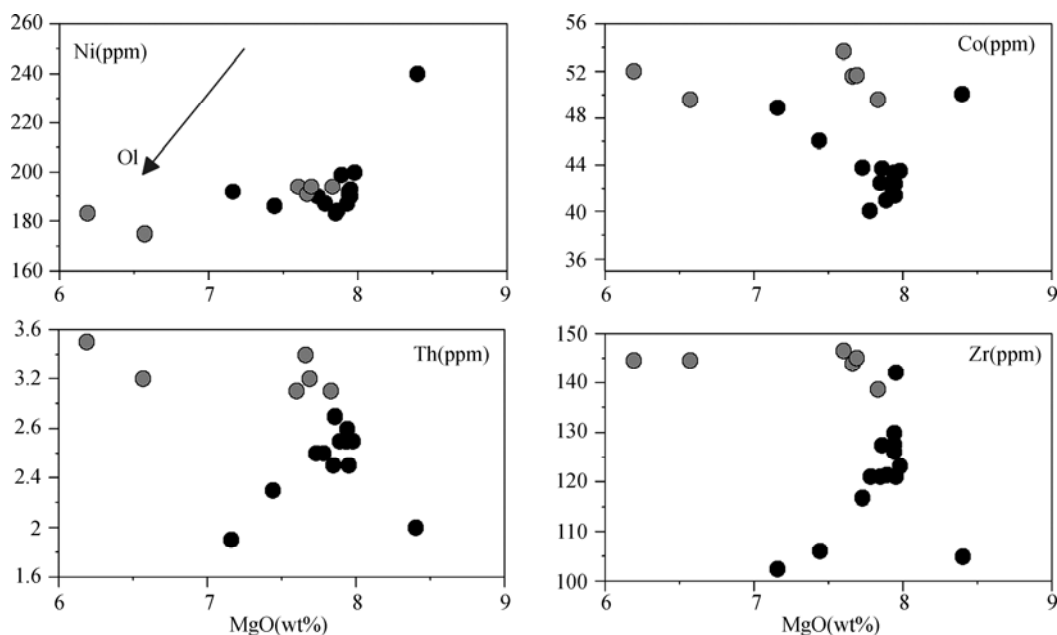


Fig. 5. Selected compatible and incompatible trace element variations plotted against MgO. References as in Figure 3.

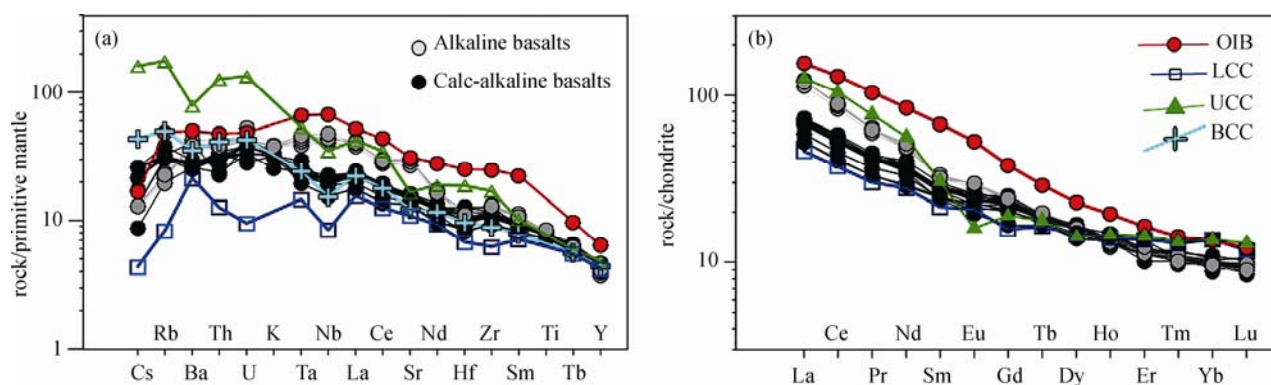


Fig. 6. Primitive-mantle (a) and chondrite (b) normalized multi-element variation diagrams for the Miocene Gaziantep Basin lavas.

Normalized values from Sun and McDonough (1989). For comparison plotted compositions of OIB (Ocean island basalts from Sun and McDonough (1989) were used; LCC (Lower continental crust), UCC (Upper continental crust), BCC (Bulk continental crust). Continental crust values from Taylor and McLennan (1985).

anomaly is found in all the rocks, and this fact indicates that no plagioclase fractionation occurs.

4.1 Sr–Nd isotopic compositions

The Sr–Nd isotope data of the studied basic lavas are given in Table 3. The primitive Sr–Nd calculations are based on the age of lavas from the study area and similar lavas found in its vicinity, that is, 16 Ma (Ilani et al., 2001; Ulu et al., 1991; Arger et al., 2000; Tatar et al., 2004; Lustrino et al., 2010; Ma et al., 2013). The Sr and Nd isotope ratios are usually similar and narrow. This feature indicates that both series of lavas are of homogenized isotopic composition. In the alkaline and calc-alkaline lavas, the initial $^{87}\text{Sr}/^{86}\text{Sr}$ isotope ratios change between 0.7036562–0.7045744 and 0.7037085–0.7055456, respectively. The Sr isotope ratios are high in the calc-alkaline lavas, but their range is very small and close to the ratios of the alkaline samples. Similarly, $^{143}\text{Nd}/^{144}\text{Nd}$ isotope ratios show similar distributions in the alkaline and calc-alkaline samples. However, one sample of each of the series (A5=0.512640, A3=0.512635) differs from the rest of the samples and shows low Nd and high Sr isotope values. The ϵNd values are similar in the alkaline and calc-alkaline samples. Specifically, the values are positive and range between 3.8 and 4.03. The ϵNd values in Nd samples A3 (0.35) and A5 (0.45) are low. These

samples differ from the rest because of their low ϵNd values. In the Sr–Nd isotopic correlation diagrams, the resemblance between the alkaline and calc-alkaline samples is clearly observed (Fig. 7). In these diagrams, the studied volcanic rocks are evaluated with the volcanism existing in their vicinity and on the Arabian Plate (Fig. 7). According to the evaluations, the alkaline and calc-alkaline rocks (except for A3 and A5) interact with the plateau basalts of the Karacadağ volcanic succession to the near east of the region (Fig. 7a). The samples found in the depleted source area and MORB region (except for A3 and A5) conform to the Neogene-aged lavas of Syria situated on the Arabian Plate and fall in the same area (except for A3 and A5) (Fig. 7b). Samples A3 and A5 are close to the Arabian upper crust data owing to their high Sr isotopic values. The different trends between A3 and A5 and other samples indicate that they may result from different petrogenetic processes similar to the lavas of the Syria–Aleppo Plateau.

Therefore, samples with high Nd isotope ratios are formed previously and are products of a highly primitive mantle source, whereas samples with low Nd isotope ratios indicate the partial melting of a relatively enriched, heterogeneous, and shallow mantle. Although high Sr isotope ratios change in direct proportion to the age of the crust, the Nd isotope ratios show a negative trend. These

Table 3 Sr- and Nd-isotope data of the Miocene lavas analyzed in this study

	Sample No	Rb (ppm)	Sr (ppm)	$^{87}\text{Rb}/^{86}\text{Sr}$	$^{87}\text{Sr}/^{86}\text{Sr}$	$^{87}\text{Sr}/^{86}\text{Sr}_i$	Nd (ppm)	Sm (ppm)	$^{143}\text{Nd}/^{144}\text{Nd}$	$^{143}\text{Nd}/^{144}\text{Nd}_i$	ϵNd
calc-alkaline basalts	A3	20.0	326	0.1776074	0.705586	0.7055456	17.6	4.06	0.512650	0.512635	0.35
	A15	20.3	338	0.1738713	0.704254	0.7042145	17.2	4.19	0.512827	0.512812	3.79
	A24	20.1	322	0.1807127	0.703884	0.7038429	16.9	4.21	0.512826	0.512810	3.76
	A26	20.5	341	0.1740396	0.703748	0.7037085	18.6	4.42	0.512839	0.512824	4.03
alkaline basalts	A5	14.5	573	0.0732592	0.704591	0.7045744	22.1	4.74	0.512654	0.512640	0.45
	A9	15.0	635	0.0683858	0.703861	0.7038455	23.1	4.91	0.512824	0.512811	3.77
	A16	14.0	629	0.0644356	0.703752	0.7037374	23.8	4.75	0.512829	0.512816	3.88
	A31	14.5	645	0.0650814	0.703671	0.7036562	22.4	4.76	0.512837	0.512824	4.02

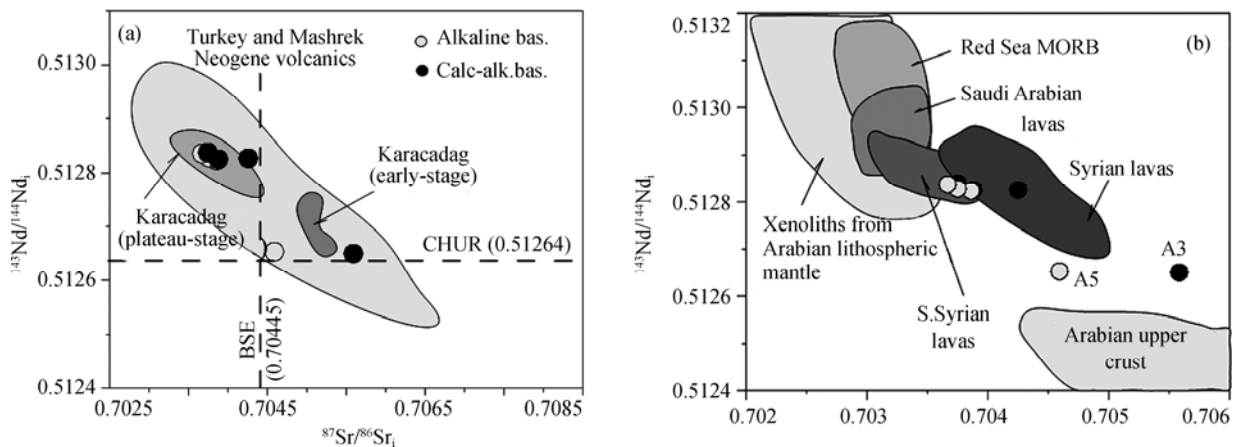


Fig. 7. $^{87}\text{Sr}/^{86}\text{Sr}_{(i)}$ vs $^{143}\text{Nd}/^{144}\text{Nd}_{(i)}$ diagram from the Gaziantep Basin volcanic rocks. Also plotted for comparison are the samples from eastern Turkey volcanic rocks and Karacadag lavas (Lustrino et al., 2010). (a), and other Tertiary to Quaternary volcanic rocks of the Arabian Plate and Syrian (alkali basalt, tholeiite, hawaiite, mugearite, basaltic andesite) lavas (Krienitz et al., 2006); (b), BSE $\frac{1}{4}$ Bulk Silicate Earth value ($^{87}\text{Sr}/^{86}\text{Sr} \frac{1}{4} 0.70445$); CHUR $\frac{1}{4}$ Chondritic Uniform Reservoir ($^{143}\text{Nd}/^{144}\text{Nd} \frac{1}{4} 0.51264$).

properties of the samples conform to those of various volcanic formations caused by tectonic structures, such as the Dead Sea Fault System and the Bitlis Suture Zone in different regions of Syria during the last 20 Ma, as indicated in previous studies (Krienitz et al., 2009).

5 Discussion

The geochemical properties of the studied alkaline and calc-alkaline lavas naturally show partial differences. The parental magma and evolution processes of these series are determined using their geochemistry and Sr–Nd isotope compositions to determine their petrogenetic properties, which are discussed in the following sections.

5.1 Crystal fractionation and partial melting process

As demonstrated in the petrographic investigations above, the existence of olivine and plagioclase phenocrystals along with pyroxene microcrystals in all the samples is important for fractionation. The major element distribution versus MgO content and the decrease in Ni with MgO content may indicate olivine, clinopyroxene, and spinel fractionation (Fig. 5a). The formation depth of basalts affects the contents of FeO^* , MgO, and SiO_2 and the silica saturation degree of the magma (Kushiro, 1996). Kushiro (1996) claimed that under pressures lower than 10 kbar the liquids that are in balance with the mantle peridotite exhibit normative hypersthene regardless of fractionation. Hypersthene is normative when nepheline is formed either under 15 kbar or high pressure and approximately less than 10% melting conditions, or under high pressure and large melting fractions (De Paolo and Daley, 2000). In the current study rocks with alkaline composition include normative nepheline whereas those

with sub-alkaline composition include hypersthene (Table 1).

The melting model of the studied samples is evaluated using the diagram designed by Shaw (1970) to derive the fractional and mass melting equations (Fig. 8a). All the samples are located on and around the FC curve and are of spinel–peridotite source (Fig. 8a). Both groups of rocks are located very closely. The samples do not display irregular distribution, and this fact indicates that the mantle source and melting process change very little in time.

The ratios of isotopes and some elements and the ratios of elements with FC or AFC processes are shown Fig. 8b–d. In the figures, the changes in $^{87}\text{Sr}/^{86}\text{Sr}_{(i)}$ isotope ratio versus Th and SiO_2 and $^{143}\text{Nd}/^{144}\text{Nd}_{(i)}$ ratio versus Sm/Nd are observed. In the diagrams, both groups of rocks display similar processes and FC creates a more effective compositional difference than that of AFC.

On the one hand, the distributions of both sample groups in such a pattern indicate fractional crystallization in various degrees; on the other hand, they predominantly indicate the fractionation of the ferromagnesian minerals. In the calc-alkaline samples in particular, the decrease in Na_2O and K_2O with MgO indicates the crystallization of Na- and K-bearing minerals, such as amphibole, biotite, Na-plagioclase, and K-feldspar. The behavior of alkaline elements, which are highly differentiated in the calc-alkaline rocks, cannot be explained by normal fractionation. Similarly, the significantly flat distribution of HREEs in the chondrite-normalized diagram reflects a moderate fractionation and lack of garnet in the source. This distribution also indicates that the main magma was formed in the lithospheric mantle (in spinel peridotite) at shallow depth. No Eu anomaly is observed in any of the

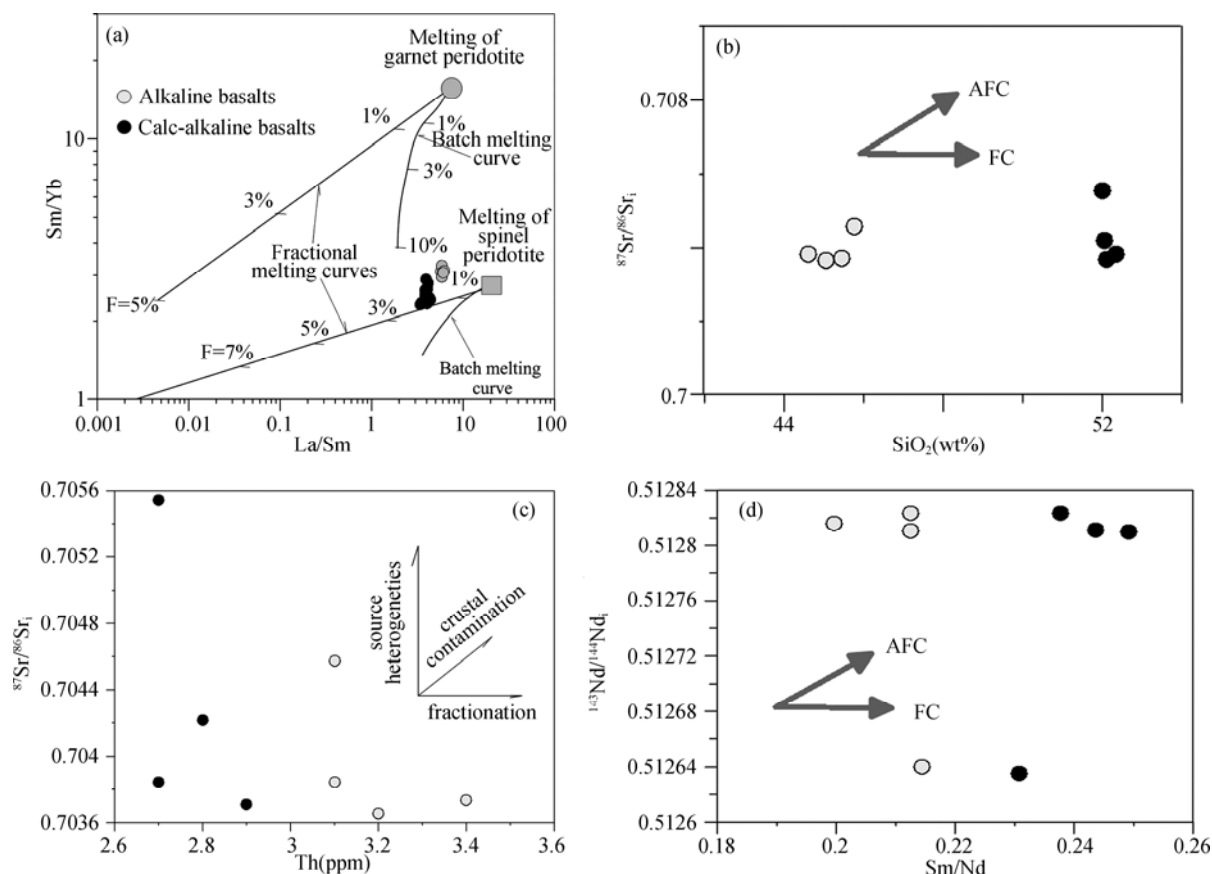


Fig. 8. (a), La/Sm vs Sm/Yb plot showing theoretical melting curves. Diagram, fractional and batch melting equations of Shaw (1970) were used to construct the melting model made by Keskin (2005) using samples taken from the Erzurum-Kars Plateau of the basic volcanic rocks ($\text{SiO}_2 < 57\%$). Modal mineralogy for the spinel- and garnet-peridotites are taken from Wilson (1989) ($\text{ol}_{.66} + \text{opx}_{.24} + \text{cpx}_{.08} + \text{sp}_{.02}$ and $\text{ol}_{.63} + \text{opx}_{.30} + \text{cpx}_{.02} + \text{gt}_{.05}$); (b), $(^{87}\text{Sr}/^{86}\text{Sr})_{(t)}$ vs SiO_2 ; (c), $(^{87}\text{Sr}/^{86}\text{Sr})_{(t)}$ vs Th; (d), $(^{143}\text{Nd}/^{144}\text{Nd})_{(t)}$ vs Sm/Nd plots showing possible fractional crystallization (FC) and/or assimilation-fractional crystallization (AFC) and source heterogeneity trends for the basaltic lava samples of the study area.

rocks, and this fact indicates that no significant plagioclase fractionation occurred.

5.2 Source characteristics and crustal contamination

Krienitz et al. (2006) found that, by using quantitative fractionation processes, the lavas in northwest Syria originate from two different magma sources (Ghiorso and Sack, 1995). Putirka et al. (1996) used the clinopyroxene-liquid thermobarometer to determine the pressure-temperature interval of crystallization (Putirka et al., 1996). The results indicated that high-P lavas are formed under 25–14 km depths and 0.7–0.4 GPa pressure conditions, whereas low-P lavas (clinopyroxene crystallization) are formed under shallow (~11 km) and ~0.3 GPa pressure conditions. Therefore, both groups of magmas are formed under the sedimentary crust (6 km) and within ~20 km depth. Alparslan (2007) observed that the melting depth of the Early-Middle Miocene basic volcanic rocks of the region changes from spinel-peridotite to garnet-peridotite areas. He also stated that the probable magma source that formed this volcanism might

have been deep lithospheric mantle or asthenosphere. All the investigated alkaline samples in the current study contain normative nepheline, whereas some other basalts contain normative hypersthene (Table 1). These results indicate that basalts originate from undepleted magma and that the alkaline basalts were formed under high pressure and low melting conditions whereas the calc-alkaline basalts formed under low pressure and high melting conditions. HFSEs, such as Nb and Ta, are depleted compared with the LREEs; therefore, the ratio of Nb/La is low in the lithospheric mantle ($\sim < 0.5$) and high ($\sim > 1$) in OIBs of asthenospheric mantle origin (Smith et al., 1999). The Nb/La ratio is high in the current studied samples of alkaline composition whereas the ratio is low (lithospheric-asthenospheric mantle transition zone) in the other samples (Fig. 9a). Alpaslan (2007) also stated that the volcanic rocks in the region are derived from two sources, namely, spinel-peridotite and garnet-peridotite, which are reflected as chemical or thermal instabilities in the morphology of olivine. He also stated that these melts of different origins started in different magma chambers but

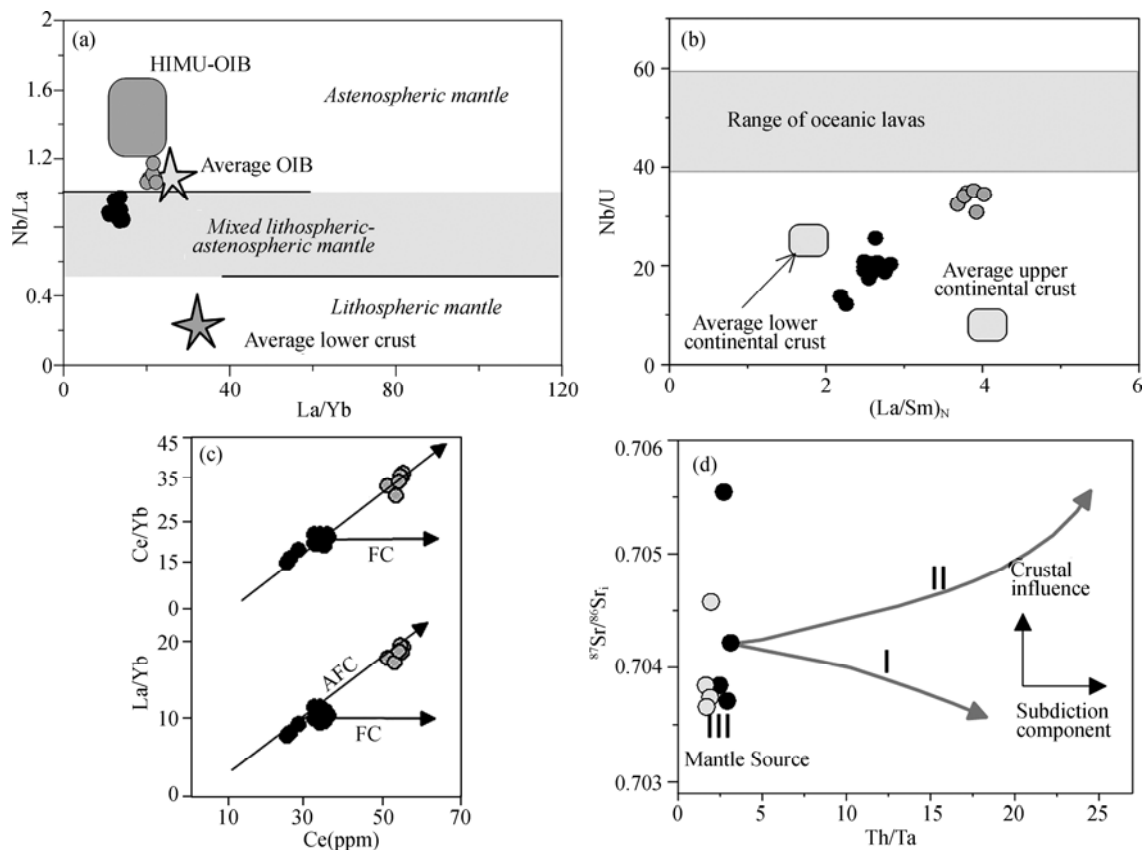


Fig. 9. (a), Plot of La/Yb vs Nb/La (Kaygusuz et al., 2011) and $(\text{La}/\text{Sm})_{\text{N}}$ vs Nb/U ; (b), (Krienitz et al., 2006) showing different trends for the two lava groups. Evolution trends of the studied basaltic lavas in the Ce vs Ce/Yb (Ajaji et al., 1998) and Ce vs La/Yb (Juteuteau and Maury, 1997); (c), diagrams. Th/Ta vs $^{87}\text{Sr}/^{86}\text{Sr}$ diagram in the studied volcanic rocks are distinguish crustal contamination and subduction influence (Kramer et al., 2005); (d), The arrows indicate possible subduction influence (I) or combined subduction and/or crustal influence (II), (III) volcanic rocks with tholeiitic tendency and OIB-type basalts. HIMU high U / Pb ratio (high μ value) mantle, OIB ocean island basalts, FC fractional crystallization, AFC assimilation fractional crystallization

then formed a single flow. By contrast, Lustrino et al. (2012) thought that the geochemical data of the Karacadağ volcanic rocks indicate that they are the products of partial melting of a chemically and mineralogical heterogeneous mantle source rather than from crustal contamination. Those researchers also stated that the materials with low temperature (e.g., amphibole and phlogopite-rich metasomes) contribute significantly to the partial melts in the early stages of mantle melting. However, the lavas found in the Aleppo Plateau of Syria, which is south of the study area, differ and conform to the high-pressure crystallization (~ 10 kbar; low crust conditions) seen in the MELTS model (thermodynamic modeling of phase equilibria in magmatic systems) (Ma et al., 2013). Ma et al. (2013) discovered that clinopyroxene is an important liquid phase and that olivine cannot crystallize under such high pressures. The optimum conditions are specified as 1 kbar (~ 3 – 4 km) for the Phase 1 basalts and 5 kbar (~ 18 km) for the Phase 2 ne-normative basalts in the lavas of Aleppo Plateau. Ma et al. (2013) also emphasized the importance of AFC processes in the evolution of the Phase

2 hy-normative basalts.

Hofmann et al. (1986) indicated that oceanic magmas derived from the upper mantle exhibit a $49\% \pm 10$ Nb/U ratio. The average UCC presents 9% Nb/U and the average LCC shows 25% Nb/U ratio (Rudnick and Fountain, 1995). According to these data, the distributions in the $(\text{La}/\text{Sm})_{\text{N}}$ -Nb/U diagram (Hofmann et al., 1986) of the studied rocks (Fig. 9b) are similar to those of rocks found in northwest Syria (Krienitz et al., 2006). Thus, the decrease in the Nb/U ratios during the magmatic differentiation of these volcanic rocks cannot be explained solely by fractionation because the differentiation of crystallized mineral phases cannot affect the behavior of these elements. Therefore, the negative correlation between SiO_2 and Nb/U indicates crustal contamination of the magma. Similarly, the positive trend in the Ce versus the Ce/Yb and La/Yb diagrams (Fig. 9c) indicates AFC in both groups of rocks. An increase in Ce content is related to crustal contamination of the most significant thickening of the crust in active margins (Juteuteau and Maury, 1997).

The ratio of Nb with respect to other elements is frequently used to indicate crustal contamination. According to Mojgan (2008), $La/Nb > 1.5$ indicates crustal contamination. In the present study, the ratio of La/Nb changes between 1.02 and 1.20 in the samples with calc-alkaline composition, whereas the ratio of La/Nb changes between 0.85 and 0.94 in the samples with alkaline composition (Table 1). Although the La/Nb ratios of all the studied samples are close to one another and of a narrow range, the crustal effect is more significant in the calc-alkaline samples than in the alkaline samples. Similarly, La/Ta ratios are also used as a contamination indicator (Fitton et al., 1988; Leat et al., 1988; Thompson and Morrison, 1988). According to Leat et al. (1988), $La/Ta < 22$ ratios indicate asthenospheric origin. Thomson and Morrison (1988) claimed that La/Ta ratios between 10 and 12 indicate asthenospheric origin and ratios >30 indicate crustal or lithospheric contamination. Accordingly, the La/Ta ratios of both groups of rocks change between 13–19% in the present study. For this reason, it can be said that these rocks are composed of uncontaminated asthenosphere mantle source (Leat et al., 1988) rather than crustal contamination (Thompson and Morrison, 1988).

In the multi-element diagrams (Fig. 6), the rocks with alkaline composition are enriched in LREEs and HFSEs. Crustal assimilation creates irregularities, particularly in the distributions of incompatible trace elements. Continental crust is characterized by highly fractionated and enriched LREEs, flat HREEs, and positive Pb (Taylor and McLennan, 1985). Similar to these data, the LREE and HFSE of the studied samples are enriched, whereas their HREEs display a flat distribution.

The isotope composition of the lavas also indicates the effects of AFC. As shown in Fig. 9d, the change in Sr isotope ratio with Th/Ta shows the importance of crustal effect in the melts of mantle origin.

The Siverek/Karacadağ Plateau basalts situated near to the east of the study area are also affected by crustal contamination (Lustrino et al., 2010; Ekici et al., 2012). Similarly, Krienitz et al. (2009) explained that the low Ce/Pb (<20) and Nb/Th (<10) ratios and Sr, Nd, and Pb isotope contents of the volcanic rocks in northwest Syria are the results of 30% crustal contamination.

5.3 Tectonic implications

The Neogene tectonic evolution of southeastern Anatolia is widely affected by the collision of the African and Arabian plates with the Eurasian Plate. The formation of DSFZ, which is defined within the same tectonic evolution, resulted in the opening of the Red Sea (Gaulier et al., 1988) and the separation and northward migration of

the Arabian Plate from Africa (Le Pichon and Gaulier, 1988). The continuing northward movement caused the ultimate collision to the north of the Arabian Plate during the Middle–Late Eocene (Hempton, 1985). The convergence that created this collision continued and led to compressional features, such as partial shortening and thickening of the Arabian continental margin (Hempton, 1985). The African–Arabian divergent plate movement and the opening of the Red Sea are the main influencing factors of the structural developments in SE Anatolia. The DSFZ, which caused the Quaternary volcanism in SE Anatolia (Parlak et al., 1998, 2000; Coşkun and Coşkun, 2000; Yürür and Chorowicz, 1998; Yüce et al., 2014), continues from the Red Sea to the Bitlis Suture Zone in the Maraş triple junction (Adıyaman and Chorowicz, 2002) (Fig. 1). The volcanism in SE Anatolia and Syria resulted from the transtensional stress generated along the DSFZ (Alpaslan, 2007; Ilani et al., 2001). Ekici et al. (2012) reported that the Siverek Plateau basalts represent the rising and melting of the mantle under the thinned or weakened Arabian Plate, which continued to move northward during the Neogene. In the same manner, the alkaline volcanism in N Syria and SE Turkey is related to the subduction and slab breakoff under the Bitlis Suture Zone (Faccenna et al., 2006). Similarly, the volcanism in W Syria and the Arabian Plate (Fig. 1) and the renewed tectonic activity may reflect the mantle rising up under the Arabian Plate to the west.

Different tectono-magmatic discrimination diagrams are used to interpret the tectonic evolution of the studied Miocene volcanic sequences on the basis of the above-mentioned tectonic elements (Fig. 10). Using the diagram ($Zr/Y-Zr$) for which less mobile HFSEs are used (Pearce and Norry, 1979), the rocks of calc-alkaline and alkaline compositions are located in the within-plate tectonic region (Fig. 10a). Similarly, in the La/10-Y/15-Nb/8 triple diagram, all the samples are located within the continental basalt area (Fig. 10b).

6 Conclusions

The Miocene continental lavas situated within the Arabian Plate in the Gaziantep Basin of SE Anatolia are of basaltic composition. These basalts present similar mineralogical composition (olivine, plagioclase, and pyroxene), contain olivine phenocrysts in different amounts, and exhibit fine- to coarse-grained texture.

Geochemical data prove that these rocks are alkaline and calc-alkaline in nature and that the alkaline rocks contain normative nepheline whereas the calc-alkaline rocks contain hypersthene. Element distributions in these rocks indicate olivine, clinopyroxene and spinel

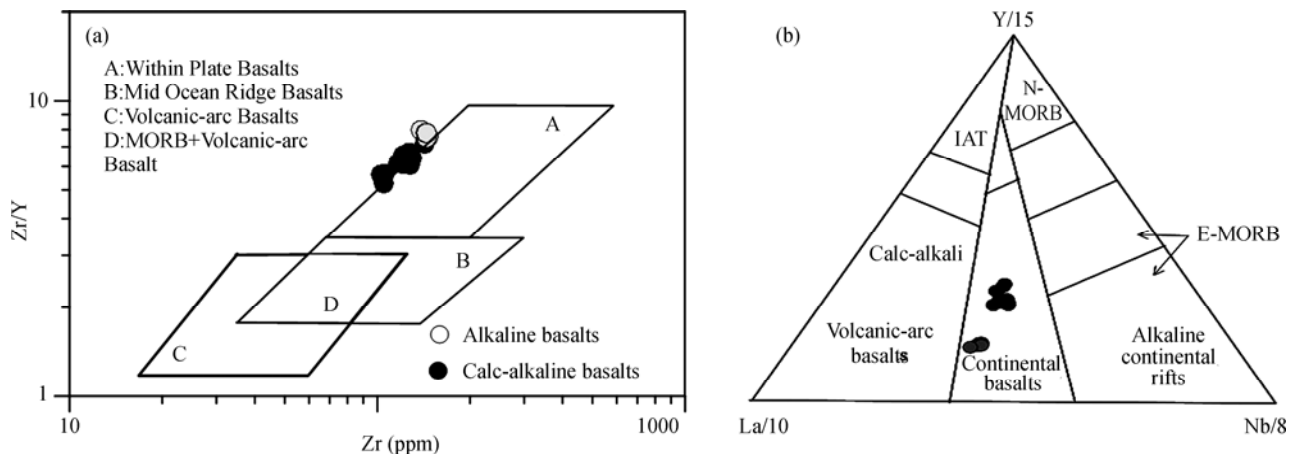


Fig. 10. Plot of the study area lavas in the tectonic discrimination diagrams. (a), Zr/Y versus Zr (Pearce and Norry, 1979); (b) Y/15-La/10-Nb/8 (Cabanis and Lecolle, 1989).

fractionation.

In the multi-element diagrams, no prominent positive and negative peaks are found. However, enrichment in LREE, Ta, Nb, and Sr in the alkaline lavas and weak Nb anomaly in the calc-alkaline lavas are observed. Despite these differences, elements of both volcanic groups are commonly conformable with BCC.

The Sr and Nd isotope compositions of the two magmas (alkaline and calc-alkaline) are similar. In addition, the behavior of isotopes with a few incompatible elements show similar trends. However, one sample in each group of rocks (calc-alkaline sample A3 and alkaline sample A5) differs in Sr and especially Nd isotope compositions. Although the Sr and Nd chemical compositions of these two samples are the same or similar to other samples, the different Sr and Nd isotope compositions may indicate a heterogeneous magma.

The trace element contents and isotopic compositions of all samples with low Mg and Ni contents support low degree partial melting and FC.

The geochemical data of these alkaline and calc-alkaline samples indicate that the mantle source that generated these lavas changed in nature and in melting process in time and that this phenomenon conforms to the heterogeneous lithosphere.

Significant crustal material contamination is not observed in the rocks that have not undergone any significant alteration processes (low Nb/U). However, Sr and Nd isotope ratios do not conform to the element ratios of both groups of studied lavas. This fact indicates that more than one entity occurs in the formation of magma. The reason is attributed to the collision of the Arabian and Eurasian plates and the development of DSFZ thereafter. Partial melting along this fault zone and melting in relation to the tectonic formations may help explain the complexity of these lavas.

As a result of all these data, the relationships of these alkaline and calc-alkaline lavas with the volcanism found in the vicinity of the study area (within the Arabian Plate) are still unclear. This volcanism cannot be correlated with either the young alkaline volcanism in the Siverek/Karacadağ Plateau basalts near to the east of the study area or the widespread alkaline and tholeiitic magmatic activity in W-NW Syria during the Eocene-Oligocene transition.

Acknowledgements

The authors would like to thank the University of Firat Scientific Research Projects Unit (FÜBAP) for research support (Project number MF-13.06). We are also grateful to editor of the *Acta Geologica Sinica* and reviewers for their comments.

Manuscript received Oct. 16, 2017

accepted Jan. 12, 2018

edited by Susan Turner and Fei Hongcai

References

- Adiyaman, O., and Chorowicz, J., 2002. Late Cenozoic tectonics and volcanism in the northwestern corner of the Arabian plate: a consequence of the strike-slip Dead Sea fault zone and the lateral escape of Anatolia. *Journal of Volcanology and Geothermal Research*, 117: 327–45.
- Ajaji, T., Weis, D., Giret, A., and Bouabdellah, M., 1998. Coeval potassic and sodic calc-alkaline series in the post-collisional Hercynian Tanncherfi intrusive complex, northeastern Morocco: geochemical, isotopic and geochronological evidence. *Lithos*, 45: 371–393.
- Allen M.B., and Armstrong, H.A., 2008. Arabia-Eurasia collision and the forcing of mid-Cenozoic global cooling. *Palaeogeography, Palaeoclimatology, Palaeoecology*, 265: 52–58
- Alpaslan, M., 2007. Early to Middle Miocene intra-continental basaltic volcanism in the northern part of the Arabian Plate,

- SE Anatolia, Turkey: Geochemistry and petrogenesis. *Geological Magazine*, 144 (5): 867–882.
- Arger, J., Mitchell, J., and Westaway, R., 2000. Neogene and Quaternary volcanism of south-eastern Turkey. In: Bozkurt, E., Winchester, J.A. and Piper, D.A. (eds.), *Tectonics and Magmatism of Turkey and the surrounding area*. Geological Society, London, Special Publications, 173: 459–487.
- Bridgland, D., Demir, T., Seyrek, A., Pringle, M., Westaway, R., Beck, A., Yurtmen, S., and Rowbotham, G., 2007. Dating Quaternary volcanism and incision by the River Tigris at Diyarbakır, SE Turkey. *Journal of Quaternary Science*, 22: 387–393.
- Cabanis, B., and Lecolle, M., 1989. Le diagramme La/10-Y/15-Nb/8: un outil pour la discrimination de series volcaniques et la mise en evidence des processus de melange et/ou de contamination crustale. *Comptes Rendus de l'Academie des Sciences*, 309: 2023–2029.
- Coşkun, B., and Coşkun, B., 2000. The Dead Sea Fault and related subsurface structures, Gaziantep Basin, southeast Turkey. *Geological Magazine*, 137: 175–192.
- Çapan, U.Z., Vidal, P., and Cantagrel, J.M., 1987. K–Ar, Nd, Sr and Pb isotopic study of Quaternary volcanism in Karasu Valley (Hatay), N-end of Dead-Sea Rift zone in SE Turkey. *Bulletin for Earth Sciences*, 14: 165–78.
- Çoban, H., 2007. Basalt magma genesis and fractionation in collision and extension related provinces: a comparison between eastern, central and western Anatolia. *Earth Science Reviews*, 80: 219–238.
- Demir, T., Westaway, R., Bridgland, D., Pringle, M., Yurtmen, S., Beck, A., and Rowbotham, G., 2007. Ar–Ar dating of late Cenozoic basaltic volcanism in northern Syria: Implications for the history of incision by the River Euphrates and uplift of the northern Arabian Platform. *Tectonics*, 26: TC3012, doi: 10.1029/2006TC001959
- De Paolo, D.J., and Daley, E.E., 2000. Neodymium isotopes in basalts of the southwest basin and range and lithospheric thinning during continental extension. *Chemical Geology*, 169: 157–185.
- Dewey, J.F., Hempton, M.R., Kidd, W.S.F., Şaroğlu, F., and Şengör, A.M.C., 1986. Shortening of continental lithosphere: The neotectonics of Eastern Anatolia—a young collision zone. In: Coward, M.P., and Ries, A.C. (eds.), *Collision Tectonics*. Geological Society, London, Special Publications, 19: 3–36.
- Dilek, Y., and Altunkaynak, S., 2009. Geochemical and temporal evolution of Cenozoic magmatism in western Turkey: Mantle response to collision, slab breakoff, and lithospheric tearing in an orogenic belt, in Van Hinsbergen. In: Edwards, D.J.J., and Govers, M.A.R. (eds.), *Collision, and Collapse at the Africa–Arabia–Eurasia Subduction Zone*. Geological Society, London Special Publications, 311: 213–233, Doi: 10.1144/SP311.8
- Ekici, T., Macpherson, C.G., and Otlu, N., 2012. Polybaric melting of a single mantle source during the Neogene Siverek phase of the Karacadağ Volcanic Complex, SE Turkey. *Lithos*, 146: 152–163.
- Faccenna, C., Bellier, O., Martinod, J., Piromallo, C., and Regard, V., 2006. Slab detachment beneath eastern Anatolia: A possible cause for the formation of the North Anatolian Fault. *Earth and Planetary Science Letters*, 242: 85–97, doi:10.1016/j.epsl.2005.11.046
- Floyd, P.A., and Winchester, J.A., 1975. Magma type and tectonic setting discrimination using immobile elements. *Earth and Planetary Science Letters*, 27: 211–218.
- Frizon de Lamotte, D., Raulin, C., Mouchot, N., Wrobel-Daveau, J.C., Blanpied, C., and Ringenbach, J.C., 2011. The southernmost margin of the Tethys realm during the Mesozoic and Cenozoic: initial geometry and timing of the inversion processes. *Tectonics*, 30: TC3002. http://dx.doi.org/10.1029/2010TC002691
- Fitton, J.G., James, D., Kempton, P.D., Ormerod, D.S., and Leeman, W.P., 1988. The role of lithospheric mantle in the generation of late Cenozoic basic magmas in the Western United States. *Journal of Petrology Special Issue*, 331–349.
- Garfunkel, Z., 1989. Tectonic setting of Phanerozoic magmatism in Israel. *Israel Journal of Earth Sciences*, 38: 51–74.
- Gaulier, J.M., Le Pichon, X., Lyberis, N., Avedik, F., Geli, L., Moretti, I., Deschamps, A., and Hafez, S., 1988. Seismic study of the crust of northern Red Sea and Gulf of Suez. *Tectonophysics*, 153: 55–88.
- Ghiorsso, M.S., and Sack, R.O., 1995. Chemical mass-transfer in magmatic processes, IV, a revised and internally consistent thermodynamic model for the interpolation and extrapolation of liquid–solid equilibria in magmatic systems at elevated temperatures and pressures. *Contributions to Mineralogy and Petrology*, 119: 197–212.
- Giannerini, G., Campredon, R., Feraud, G., and Abou Zakhem, B., 1988. Déformations intraplaques et volcanisme associé: exemple de la bordure NW de la plaque arabe au Cénozoïque. *Bulletin de la Société de Géologie de France*, 8: 937–947.
- Göncüoğlu, M.C., 2010. Introduction to the geology of Turkey: Geodynamic evolution of the Pre-Alpine and Alpine terranes. *General Directorate of Mineral Research and Exploration*, Ankara, 66.
- Göncüoğlu, M.C., Kozlu, H., and Dirik, K., 1997. Pre-Alpine and Alpine terranes in Turkey: Explanatory notes to the terrane map of Turkey. *Annales Géologiques des Pays Helléniques*, 37: 515–536.
- Harris, C., Marsh, J.S., and Milner, S.C., 1999. Petrology of the alkaline core of the Messum igneous complex, Namibia: evidence for the progressively decreasing effect of crustal contamination. *Journal of Petrology*, 40 (9): 1377–1397.
- Heimann, A., and Ron, H., 1993. Geometrical changes of plate boundaries along part of the northern Dead Sea transform: geochronologic and paleomagnetic evidence. *Tectonics*, 12: 477–491.
- Hempton, M., 1985. Structure and deformation of the Bitlis Suture near Lake Hazar, southeastern Turkey. *Geological Society of America Bulletin*, 96: 233–243.
- Hofmann, A.W., Jochum, K.P., Seufert, M., and White, M.W., 1986. Nb and Pb in oceanic basalts: new constraints on mantle evolution. *Earth and Planetary Science Letters*, 79: 33–45.
- Ilani, S., Harlavan, Y., Tarawneh, K., Rabba, I., Weinberger, R., Ibrahim, K., Peltz, S., and Steinitz, G., 2001. New K–Ar ages of basalts from the Harrat Ash Shaam volcanic field in Jordan: implications for the span and duration of the upper-mantle upwelling beneath the western Arabian Plate. *Geology*, 29: 171–174.
- Juteuteau, T., and Maury, R., 1997. *Geologie de la Croûte Oceanique: Petrologie et dynamique Endogene*. Paris: Editions Masson, 365.
- Kaygusuz, A., Aslan, Z., Siebel, W., and Şen, C., 2011.

- Geochemical and Sr-Nd isotopic characteristics of post-collisional calc-alkaline volcanics in the Eastern Pontides (NE Turkey). *Turkish Journal of Earth Sciences*, 20: 137–159.
- Keskin, M., 2005. Domal uplift and volcanism in a collision zone without a mantle plume: Evidence from Eastern Anatolia. <https://www.researchgate.net/publication/241329729>.
- Köksal, S., and Göncüoğlu, M.C., 2008. Sr and Nd isotopic characteristics of some S-, I- and A-type granitoids from central Anatolia. *Turkish Journal of Earth Sciences*, 17: 111–127.
- Kramer, W., Siebel, W., Romer, R.L., Haase, G., Zimmer, M., and Ehrlichmann, R., 2005. Geochemical and isotopic characteristics and evolution of the Jurassic volcanic arc between Arica (181300S) and Tocopilla (221S), North Chilean Coastal Cordillera. *Chemie der Erde*, 65: 47–78.
- Krienitz, M.S., Haase, K.M., Mezger, K., Eckardt, V., and Shaikh-Mashail, M.A., 2006. Magma genesis and crustal contamination of continental intraplate lavas in Northwestern Syria. *Contributions to Mineralogy and Petrology*, 151: 698–716.
- Krienitz, M.S., Haase, K.M., Mezger, K., Van den Bogard, P., Thiemann, V., and Shaikh-Mashail, M.A., 2009. Tectonics events, continental intraplate volcanism, and mantle plume activity in northern Arabia: Constraints from geochemistry and Ar-Ar dating of Syrian lavas. *Geochemistry Geophysics Geosystems*, 10, Q04008, doi:10.1029/2008GC002254.
- Kushiro, I., 1996. Partial melting of a fertile mantle peridotite at high pressure and experimental study using aggregates of diamond. In: Basu, A., and Hart, S. (eds.), *Earth Processes: Reading the Isotopic Code*. Geophysical Monograph Series, 95: 109–22, Washington, DC: Am. Geophys. Union.
- Kuşçu, İ., Gençaliğlu-Kuşçu, G., Tosdal, R.M., Ulrich, T.D., and Friedman, R., 2010. Magmatism in the southeastern Anatolian orogenic belt: transition from arc to post-collisional setting in an evolving orogen. In: Stephenson, R.A., Kaymakçı, N., Sosson, M., Starostenko, V. and Bergerat, F. (eds.), *Sedimentary basin tectonics from the Black Sea and Caucasus to the Arabian Platform*. Geological Society, London, Special Publications, 340: 437–460.
- Lai, S., 2016. Genesis of the Cenozoic sodic alkaline basalt in the Xiahe–Tongren area of the northeastern Tibetan Plateau and its continental dynamic implications. *Acta Geologica Sinica* (English Edition), 90(3) 1047–1048.
- Le Bas, M., Le Maitre, R.W., Streckeisen, A., and Zanettin, B., 1986. A chemical classification of volcanic rocks based on the total alkali-silica diagram. *Journal of Petrology*, 27: 745–50.
- Leat, P.T., Thompson, R.N., Morrison, M.A., Hendry, G.D., and Dickin, A.P., 1988. Compositionally diverse Miocene-recent rift related magmatism in northwest Colorado: partial melting and mixing of mafic magmas from 3 different asthenospheric and lithospheric mantle sources. *Journal of Petrology, Special Volume Issue*, 1: 351–377.
- Le Pichon, X., and Gaulier, J.M., 1988. The rotation of Arabia and the Levant Fault system. *Tectonophysics*, 153: 271–94.
- Lustrino, M., and Sharkov, E., 2006. Neogene volcanic activity of western Syria and its relationship with Arabian Plate kinematics. *Journal of Geodynamics*, 42: 115–139.
- Lustrino, M., and Wilson, M., 2007. The circum-Mediterranean anorogenic Cenozoic igneous province. *Earth-Science Reviews*, 81: 1–65.
- Lustrino, M., Keskin, M., Mattioli, M., Lebedev, V.A., Chugaev, A., Sharkov, E., and Kavak, O., 2010. Early activity of the largest Cenozoic shield volcano in the circum-Mediterranean area: Mt. Karacadağ, SE Turkey. *European Journal of Mineralogy*, 22: 343–362.
- Lustrino, M., Keskin, M., Mattioli, M., and Kavak, O., 2012. Heterogeneous mantle sources feeding the volcanic activity of Mt. Karacadağ (SE Turkey). *Journal of Asian Earth Sciences*, 46: 120–139.
- Ma, G.S.K., Malpas, J., Suzuki, K., Lo, C.H., Wang, K.L., Iizuka, Y., and Xenophontos, C., 2013. Evolution and origin of the Miocene intraplate basalts on the Aleppo Plateau, NW Syria. *Chemical Geology*, 335: 149–171.
- McQuarrie, N., Stock, J.C., Verdel, C., and Wernicke, B.P., 2003. Cenozoic evolution of Neotethys and implications for the causes of plate motions. *Geophysical Research Letters*, 30 (20): 2036. doi:10.1029/2003GL017992.
- Moix, P., Beccaletto, L., Kozur, H.W., Hochard, C., Rosselet, F., and Stampfli, G.M., 2008. A new classification of the Turkish terranes and sutures and its implications for the paleotectonic history of the region. *Tectonophysics*, 451: 7–39.
- Mojgan, S., 2008. Petrology, geochemistry and mineral chemistry of extrusive alkalic rocks of the southern Caspian Sea ophiolite, northern Alborz, Iran: evidence of alkaline magmatism in Southern Eurasia. *Journal Application Science*, 8: 2202–2216.
- MTA (General Directorate of Mineral Research and Exploration), 2002. *Diyarbakır and Hatay sheet of the geological map of Turkey, 1/500 000 scale*. Ankara.
- Okay, A.I., 2008. Geology of Turkey: A synopsis. *Anschmitt*, 21: 19–42.
- Parlak, O., Kop, A., Ünlügenç, U.C., and Demirkol, C., 1998. Geochemistry and geochronology of basaltic rocks in the Karasu graben around Kırıkkhan (Hatay), Southern Turkey. *Turkish Journal of Earth Sciences*, 7(2): 53–61.
- Parlak, O., Delaloye, M., Kozlu, H., and Fontignie, D., 2000. Trace element and Sr-Nd isotope geochemistry of the alkali basalts observed along the Yumurtalık Fault (Adana) in southern Turkey. *Bulletin for Earth Sciences*, 22: 137–148.
- Pearce, J.A., 1983. The role of sub-continental lithosphere in magma genesis at destructive plate margins. In: Hawkesworth, C.J., and Norry, M.J. (eds.), *Continental basalts and mantle xenoliths*, Nantwich, Cheshire: Shiva Publications, 230–249.
- Pearce, J.A., and Norry, M.J., 1979. Petrogenetic implications of Ti, Zr, Y, and Nb. Variations in volcanic rocks: *Contributions to Mineralogy and Petrology*, 69: 33–37.
- Perinçek, D., 1979. The geology of Hazro-Korudağ-Çüngüş-Maden-Ergani-Hazar-Elazığ-Malatya region: guide book. *Geological Society of Turkey, Special Publication*, 34.
- Ponikarov, V.P., Protasevich, L., Maximov, A., and Tkachev, G., 1963. *Geological map of Syria*. Scale 1:200,000. Moscow: V.O. Technoexport.
- Putirka, K., Johnson, M., Kinzler, R., Longhi, R., and Walker, D., 1996. Thermobarometry of mafic igneous rocks based on clinopyroxene-liquid equilibria, 0–30 kbar. *Contributions to Mineralogy and Petrology*, 123: 92–108.
- Rojay, B., Heimann, A., and Toprak, V., 2001. Neotectonic and volcanic characteristics of the Karasu fault zone (Anatolia, Turkey): The transition zone between the Dead Sea Transform and the East Anatolian Fault Zone. *Geodinamica Acta*, 14(1–3): 197–212.
- Rudnick, R.L., and Fountain, D.M., 1995. Nature and

- composition of the continental crust: a lower crustal perspective. *Reviews of Geophysics*, 33: 267–309.
- Rukieh, M., Trifonov, V.G., Dodonov, A.E., Minini, H., Ammar, O., Ivanova, T.P., Zaza, T., Ysef, A., Alshara, M., and Jobaili, Y., 2005. Neotectonic map of Syria and some aspects of Late Cenozoic evolution of the northwestern boundary zone of the Arabian Plate. *Journal of Geodynamics*, 40: 235–56.
- Shaw, D.M., 1970. Trace element fractionation during anatexis, *Geochimica Cosmochimica Acta*, 34: 237–243.
- Smith, E.I., Sanchez, A., Walker, J.D., and Wang, K., 1999. Geochemistry of mafic magmas in the Hurricane volcanic field, Utah: implications for small- and large-scale chemical variability of the lithospheric mantle. *Journal of Geology*, 107: 433–448.
- Stampfli, G.M., 2000. Tethyan oceans. In: Bozkurt, E., Winchester, J.A., and Piper, J.D. (eds.), *Tectonics and Magmatism in Turkey and the Surrounding Area*. Geological Society, London, Special Publications 173: 1–23.
- Sun, S.S., and McDonough, W.F., 1989. Chemical and isotopic systematics of oceanic basalts: implications for mantle composition and processes. In: Saunders, A.D., and Norry, M.J. (eds.), *Magmatism in the Ocean Basins*. Geological Society of London Special Publication, 42: 313–345.
- Şengör, A.M.C., and Kidd, W.S.F., 1979. Post-collisional tectonics of the Turkish–Iranian Plateau and a comparison with Tibet. *Tectonophysics*, 55: 361–376.
- Şengör, A.M.C., Görür, N., and Şaroğlu, F., 1985. Strike-slip faulting and related basin formation in zones of tectonic escape: Turkey as a case study, strike-slip deformation, basin formation, and sedimentation. *The Society of Economic Paleontologists and Mineralogists (SEPM), Special Publication*, 37: 227–264.
- Şengör, A.M.C., and Yılmaz, Y., 1981. Tethyan Evolution of Turkey: A plate tectonic approach. *Tectonophysics*, 75: 181–241.
- Tatar, O., Piper, J.D.A., Gürsoy, H., Heimann, A., and Koçbulut, F., 2004. Neotectonic deformation in the transition zone between the Dead Sea Transform and the East Anatolian Fault Zone, southern Turkey: a palaeomagnetic study of the Karasu Rift Volcanism. *Tectonophysics*, 385: 17–43.
- Taylor, S.R., and McLennan, S.M., 1985. *The Continental crust: Its composition and evolution*. Oxford: Blackwell Scientific Publications, 312.
- Taymaz, T., Yılmaz, Y., and Dilek, Y., 2007. The geodynamics of the Aegean and Anatolia: introduction. In: Taymaz, T., Yılmaz, Y. and Dilek, Y. (eds.), *The Geodynamics of the Aegean and Anatolia*. Geological Society, London, Special Publications, 291: 1–16.
- Thompson, R.N., and Morrison, M.A., 1988. Asthenospheric and lower lithospheric mantle contributions to continental extensional magmatism: An example from the British Tertiary Province. *Chemical Geology*, 68: 1–15.
- Ulu, Ü., Ercan, T., Genç, Ş.C., Metin, Y., Çörekçiöğlu, E., Örcen, S., Karabıyıköğlu, M., Giray, S., and Yaşar, T., 1991. Geology of the Nizip–Yavuzeli–Araban–Belveren district (Gaziantep, SE Anatolia) and petrology and regional distribution of the Cenozoic volcanic rocks. *Bulletin of Geological Congress of Turkey*, 6: 207–227.
- Wilson, M., 1989. *Igneous petrogenesis: a global tectonic approach*. London: Unwin Hyman, 466.
- Winchester, J., and Floyd, P.A., 1977. Geochemical discrimination of different magma series and their differentiation products using immobile elements. *Chemical Geology*, 20: 325–43.
- Yiğitbaş, E., and Yılmaz, Y., 1996. New evidence and solution to the Maden complex controversy of the southeast Anatolian orogenic belt (Turkey). *Geologische Rundschau*, 85: 250–263.
- Yılmaz, Y., 1993. New evidence and model on the evolution of the southeast Anatolian orogen. *Geological Society of America Bulletin*, 105: 251–271.
- Yılmaz, Y., Şaroğlu, F., and Güner, Y., 1987. Initiation of the neomagmatism in East Anatolia. *Tectonophysics*, 134: 177–199.
- Yurtmen, S., Rowbotham, G., Isler, F., and Floyd, P.A., 2000. Petrogenesis of basalts from southern Turkey: the Plio-Quaternary volcanism to the north of Iskenderun Gulf. In: Bozkurt, E., Winchester, J.A., and Piper, J.D.A. (eds.), *Tectonics and Magmatism in Turkey and the Surrounding Area*. Geological Society, London, Special Publications, 173: 489–512.
- Yüce, G., Italiano, F., D'Alessandro, W., Yalcin, T.H., Yasin, D.U., Gülbay, A.H., Özyurt, N.N., Rojay, B., Karabacak, V., Bellomo, S., Brusca, L., Yang, T., Fu, C.C., Lai, C.W., Özacar, A., and Walia, V., 2014. Origin and interactions of fluids circulating over the Amik Basin (Hatay, Turkey) and relationships with the hydrologic, geologic and tectonic settings. *Chemical Geology*, 388: 23–39.
- Yürür, T.M., and Chorowicz, J., 1998. Recent volcanism, tectonics and plate kinematics near the junction of the African, Arabian and Anatolian plates in the Eastern Mediterranean. *Journal of Volcanology and Geothermal Research*, 85: 1–15.

About the first author

KÜRÜM Sevcan; female, born in 1962 in Elazığ city, Turkey; she is now associate professor at Firat University, Turkey. Email: skurum@firat.edu.tr; phone: 0905327129070